The Journal of Immunology

Soluble Uric Acid Is an Intrinsic Negative Regulator of Monocyte Activation in Monosodium Urate Crystal–Induced Tissue Inflammation

Qiuyue Ma, Mohsen Honarpisheh, Chenyu Li, Markus Sellmayr, Maja Lindenmeyer, Claudia Böhland, Paola Romagnani, Hans-Joachim Anders and Stefanie Steiger

J Immunol 2020; 205:789-800; Prepublished online 19 June 2020;
doi: 10.4049/jimmunol.2000319
http://www.jimmunol.org/content/205/3/789

The Journal of Immunology is published twice each month by
The American Association of Immunologists, Inc.,
1451 Rockville Pike, Suite 650, Rockville, MD 20852

Print ISSN: 0022-1767 Online ISSN: 1550-6606.

Soluble Uric Acid Is an Intrinsic Negative Regulator of Monocyte Activation in Monosodium Urate Crystal–Induced Tissue Inflammation

Qiuyue Ma,* Mohsen Honarpisheh,* Chenyu Li,* Markus Sellmayr,* Maja Lindenmeyer,*,† Claudia Böhland,‡ Paola Romagnani,§ Hans-Joachim Anders,*,1 and Stefanie Steiger*,1

Although monosodium urate (MSU) crystals are known to trigger inflammation, published data on soluble uric acid (sUA) in this context are discrepant. We hypothesized that diverse sUA preparation methods account for this discrepancy and that an animal model with clinically relevant levels of asymptomatic hyperuricemia and gouty arthritis can ultimately clarify this issue. To test this, we cultured human monocytes with different sUA preparation solutions and found that solubilizing uric acid (UA) by prewarming created erroneous results because of UA microcrystal contaminants triggering IL-1β release. Solubilizing UA with NaOH avoided this artifact, and this microcrystal-free preparation suppressed LPS- or MSU crystal–induced monocyte activation, a process depending on the intracellular uptake of sUA via the urate transporter SLC2A9/GLUT9. $CD14^+$ monocytes isolated from hyperuricemic patients were less responsive to inflammatory stimuli compared with monocytes from healthy individuals. Treatment with plasma from hyperuricemic patients impaired the inflammatory function of $CD14^+$ monocytes, an effect fully reversible by removing sUA from hyperuricemic plasma. Moreover, Alb-creERT2;*Glut9*$^{lox/lox}$ mice with hyperuricemia (serum UA of 9–11 mg/dl) showed a suppressed inflammatory response to MSU crystals compared with *Glut9*$^{lox/lox}$ controls without hyperuricemia. Taken together, we unravel a technical explanation for discrepancies in the published literature on immune effects of sUA and identify hyperuricemia as an intrinsic suppressor of innate immunity, in which sUA modulates the capacity of monocytes to respond to danger signals. Thus, sUA is not only a substrate for the formation of MSU crystals but also an intrinsic inhibitor of MSU crystal–induced tissue inflammation. *The Journal of Immunology*, **2020, 205: 789–800.**

Uric acid (UA) is a metabolite breakdown product of purines and primarily excreted by the kidneys. In most mammals, including rodents, serum UA concentrations are low owing to the presence of the enzyme uricase, which degrades soluble UA (sUA) into the more–water soluble allantoin (1). However, humans lack functional uricase; thus, sUA is the final end product of the purine metabolism (2). As a consequence, serum UA levels are relatively high in humans and increase the risk for developing gouty arthritis or kidney stones. The excretion of sUA is largely regulated by urate transporters in the renal tubules, such as urate transporter 1 (SLC22A12/URAT1) (3, 4), glucose transporter 9 (SLC2A9/GLUT9) (5), ATP-binding cassette transporter subfamily G member 2 (ABCG2) (6), and organic anion transporters (7, 8). Hence, genetic variants, environmental factors, use of drugs that impair the UA transport capacity, and a reduced number of nephrons are frequent causes for hyperuricemia (HU) in humans (8).

sUA is the substrate for the formation of monosodium urate (MSU) crystals during gouty arthritis (9, 10). MSU crystals like many other crystals or microparticles elicit acute inflammation characterized by secretion of proinflammatory mediators, the recruitment of leukocytes from the bloodstream into the inflamed joint (11–14), and the release of neutrophil extracellular traps (12, 15, 16). Although no doubt exists on the inflammatory effects of MSU crystals, published data on the pathophysiological role of sUA remain controversial. Several in vitro studies reported proinflammatory effects of sUA, including activation of the Akt-PRAS40 pathway (17), induction of NLRP3 inflammasome-mediated IL-1β release (18–21) in immune cells, and reactive oxygen species production (22), or NF-κB and MAPK signaling in nonimmune cells (23–26). In contrast, sUA can exert antioxidant properties (8) and act as an inhibitor of protein nitrosation, lipid and protein peroxidation, low-density lipoprotein oxidation, and a deactivator of tetrahydrobiopterin (8), which were shown to elicit protective effects in neurodegenerative diseases (27) and cancer

*Division of Nephrology, Department of Medicine IV, Hospital of the Ludwig Maximilian University of Munich, 80336 Munich, Bavaria, Germany; †III. Department of Medicine, University Medical Center Hamburg-Eppendorf, 20246 Hamburg, Germany; ‡Department of Radiation Oncology, Hospital of the Ludwig Maximilian University of Munich, 80336 Munich, Germany; and §Department of Biomedical Experimental and Clinical Sciences "Maria Serio," University of Florence, 50139 Florence, Italy

[1]H.-J.A. and S.S. contributed equally.

ORCIDs: 0000-0003-3002-7442 (M.H.); 0000-0002-5402-584X (C.L.); 0000-0002-5990-494X (S.S.).

Received for publication March 25, 2020. Accepted for publication May 27, 2020.

This work was supported by grants from the Deutsche Forschungsgemeinschaft (STE2437/2-1 to S.S; AN372/14-3, 16-2, and 24-1 to H.-J.A) and LMUexcellent initiative (to S.S.).

S.S. and H.-J.A. designed the study concept and experiments. Q.M. and S.S. conducted experiments and analyzed data. M.H. assisted with technical support for siRNA experiments. M.S., M.L., C.L., and C.B. provided reagents/cells and acquired experimental data. P.R. provided the human renal progenitor cells. S.S., Q.M., and H.-J.A. wrote the manuscript. All contributing authors reviewed the manuscript.

This work was included in the Ph.D. thesis of Q.M. as presented to the Medical Faculty of the Ludwig Maximilian University of Munich, December 4, 2019, Munich, Germany.

Address correspondence and reprint requests to Dr. Stefanie Steiger, Department of Medicine IV, Hospital of the Ludwig Maximilian University of Munich, Ziemssenstrasse 1, 80336 Munich, Bavaria, Germany. E-mail address: stefanie.steiger@med.uni-muenchen.de

The online version of this article contains supplemental material.

Abbreviations used in this article: CKD, chronic kidney disease; D-PBS, Dulbecco PBS; HU, hyperuricemia; MSU, monosodium urate; NaOH, sodium hydroxide; qRT-PCR, quantitative RT-PCR; siRNA, small interfering RNA; sUA, soluble UA; UA, uric acid.

(28). In addition, sUA can inhibit Akt phosphorylation in endothelial cells (29) and modulate the activity of extracellular superoxide dismutase in atherosclerotic vessels (30).

Why do such discrepancies on the effects of sUA exist? One explanation could be the different preparation methods used in in vitro studies. Indeed, among several preparation methods, preparing sUA by prewarming or by sodium hydroxide (NaOH) solubilization are most frequently employed. We hypothesized that UA crystal contaminations may account for the false-positive reporting proinflammatory effects and that only preparing crystal-free sUA can ultimately reveal its impact on innate immunity. We speculated on immunomodulatory effects in human monocytes through the intracellular uptake of sUA in vitro, and, if so, asymptomatic HU would suppress MSU crystal–induced tissue inflammation in vivo.

Materials and Methods

Animal studies

All animal experiments were performed in accordance with the European protection law of animal welfare and upon approval by the local government authorities (Regierung von Oberbayern, reference number: ROB-55.2-2532.Vet_02-15-189) based on the European Union directive for the Protection of Animals Used for Scientific Purposes (2010/63/EU) and reported according to the Animal Research: Reporting of In Vivo Experiments guidelines (31). Mice were housed in groups of five in filter-top cages with unlimited access to food and water. Cages, nest lets, food, and water were sterilized by autoclaving before use.

Mouse model of HU

Six-week-old Alb-creERT2;*Glut9*$^{lox/lox}$ and *Glut9*$^{lox/lox}$ control mice (kindly provided by Frédéric Preitner and Bernhard Thorens, University of Lausanne, Lausanne, Switzerland) were injected i.p. with tamoxifen every alternate day for 1 wk to eliminate hepatic *Glut9* expression in Alb-creERT2;*Glut9*$^{lox/lox}$ mice (32). Both groups of mice received a standard chow diet enriched with 25.6 g of inosine per kilogram (Ssniff, Soest, Germany) to induce asymptomatic HU in Alb-creERT2;*Glut9*$^{lox/lox}$ mice for 22 d. *Glut9*$^{lox/lox}$ mice served as controls (healthy).

Air pouch model of acute MSU crystal–induced tissue inflammation

Alb-creERT2;*Glut9*$^{lox/lox}$ and *Glut9*$^{lox/lox}$ mice were injected s.c. with MSU crystals (5 mg per mouse; Invivogen, San Diego, CA) or vehicle into a preexisting air pouch, a mouse model of tissue inflammation (33). After 12 h, both groups of mice (healthy and HU) were euthanized, and air pouch fluids were collected for further analysis.

Assessment of kidney injury, inflammation, and fibrosis

Upon sacrifice, we sampled the kidneys from healthy and HU mice. We kept one kidney in RNA later solution at −80°C for RNA isolation, and the second kidney was fixed in 4% formaldehyde to be embedded in paraffin for histology analysis (34). For demonstrating kidney injury, we stained 2-μm-thick kidney sections with periodic acid–Schiff reagent. The RNA extraction kit from Qiagen (Düsseldorf, Germany) was used to isolate total RNA from mouse kidneys (n = 5 mice per group) following the manufacturer's instructions. RNA quality was assessed using 1% agarose gels before being transcribed into cDNA using reverse transcriptase (Superscript II) (Invitrogen, Carlsbad, CA). Real-time RT-PCR was performed using SYBRGreen PCR master mix and analyzed with a Light Cycler 480 (Roche, Mannheim, Germany). All gene expression values were normalized using *18s rRNA* as a housekeeping gene (35). All murine primers used for amplification were purchased from Metabion (Martinsried, Germany) and are listed in Table I.

Flow cytometric analysis of murine samples from air pouch

Air pouch fluid was harvested by injecting 1 ml of cold PBS into the air pouch. Air pouch extracts were retrieved and centrifuged at 1200 rpm for 5 min. Supernatants were collected and stored at −20°C for further cytokine and chemokine analysis by ELISA. Air pouch extracts were resuspended in wash buffer and FcR blocked for 5 min before staining with the surface Abs FITC anti-mouse Ly6G, PE anti-mouse Ly6C, and PerCP anti-mouse CD45 (all Abs obtained from BioLegend, Fell, Germany) for 30 min. After incubation, cells were washed in Dulbecco PBS (D-PBS) and reconstituted in 1 ml of fresh wash buffer (0.1% BSA, 0.01% sodium azide in D-PBS). Flow cytometry was performed using the BD FACSCalibur (Becton Dickinson, Franklin Lakes, NJ) and data analyzed with the software FlowJo 8.7 (Tree Star, Ashland, OR). AccuCheck counting beads (Thermo Fisher Scientific, Langenselbold, Germany) were used, and the absolute number of cells per microliter was calculated according to manufacturers' instruction.

Assessment of mouse kidney injury

Serum blood urea nitrogen and creatinine (DiaSys, Holzheim, Germany) and serum UA (BioAssay Systems, Hayward, CA) levels were measured using commercially available kits as per manufacturer's protocol.

Isolation of human CD14$^+$ monocytes

Human PBMCs were isolated from healthy individuals (n = 8; plasma UA: 4.17 ± 0.46 mg/dl; plasma urea: 28.26 ± 3.83 mg/dl; plasma creatinine: 1.45 ± 0.05 mg/dl) or hyperuricemic chronic kidney disease (CKD) patients stage G2–5 (n = 10; plasma UA: 9.73 ± 0.5 mg/dl; plasma urea: 85.65 ± 8.35 mg/dl; plasma creatinine: 5.5 ± 0.53 mg/dl) using an S-Monovette with lithium-heparin-gel (SARSTEDT, Nümbrecht, Deutschland), followed by standard dextran sedimentation and Ficoll–Hypaque density centrifugation procedures (36). We only included patients that did not receive immunosuppressive drugs and urate-lowering therapy. CD14$^+$ monocytes were purified by magnetic activated cell sorting with human CD14 microbeads for positive selection (Miltenyi Biotec, Bergisch Gladbach, Germany), according to manufacturers' protocol. Monocytes (1×10^6 cells/ml) were suspended in complete RPMI medium (10% FBS, 1% penicillin/streptomycin, pH 7.4) and seeded onto 24-well plates in a 5% carbon dioxide atmosphere at 37°C for 30 min before stimulation. The study to obtain whole blood samples from healthy individuals and hyperuricemic CKD patients was approved by the local Ethical Review Board of the Medical Faculty at the Hospital of the Ludwig Maximilian University of Munich. Informed consent was obtained from all subjects prior to inclusion in the study.

Preparation of UA

Two methods described in the literature were used. First, UA (Sigma-Aldrich, Taufkirchen, Germany) was solubilized at different concentrations in prewarmed RPMI media, mixed, and incubated at 37°C for 1 h. After incubation, pH was checked, and all sUA solutions were filtered sterile using a 0.22-μm filter (17, 18, 22, 37, 38). Second, UA (25 mg) was solubilized by adding 50 ml of prewarmed RPMI medium, and 4 N of NaOH (50 μl) was added. The UA solution was mixed to dissolve crystals. Afterwards, pH was adjusted to 7.2 with 6 N of HCl (35 μl), the UA stock solution was mixed and filtered sterile (0.22-μm filter) (39). The concentration of the UA solutions (5–50 mg/dl) was measured, and the presence of UA microcrystals was visualized under the light microscope. For all in vitro cell culture experiments with CD14$^+$ monocytes and THP-1 cells, we used freshly prepared UA solubilized with NaOH apart from data presented in Fig. 1C and 1H.

Human CD14$^+$ monocyte stimulation assay

CD14$^+$ monocytes were isolated from healthy individuals or hyperuricemic patients and pretreated with or without 10 mg/dl sUA or 20% human plasma from healthy individuals or HU patients (with or without 0.1 μg/ml rasburicase) and then stimulated either with 10 μg/ml LPS (Sigma-Aldrich) or 500 μg/ml MSU crystals (InvivoGen) or left untreated (medium control). Total mRNA was isolated for RT-PCR after 4 h, cells were prepared for intracellular cytokine staining after 8 h of stimulation by flow cytometry, or supernatants were collected for neutrophil extracellular trap formation assays.

For intracellular staining, CD14$^+$ monocytes from healthy individuals were incubated with brefeldin A for 15 min. Cells were then harvested, washed, and resuspended in cell fixation/permeabilization buffer (BD Cytofix/Cytoperm Solution Kit; Thermo Fisher Scientific) for 15 min and washed in permwash buffer (BD Cytofix/Cytoperm Solution Kit; Thermo Fisher Scientific). Intracellular Abs for anti-human TNF-α and anti-human IL-6 (BioLegend) were added for 40 min at 4°C. After incubation, cells were washed with D-PBS and reconstituted in fresh wash buffer (0.1% BSA, 0.01% sodium azide in D-PBS). Flow cytometry was performed using the BD FACSCalibur (Becton Dickinson) and analyzed using FlowJo 8.7 (Tree Star).

Cell culture and stimulation of human monocytic THP-1 cells

Human monocytic THP-1 cell line was purchased from American Type Culture Collection and grown in RPMI culture medium supplemented with

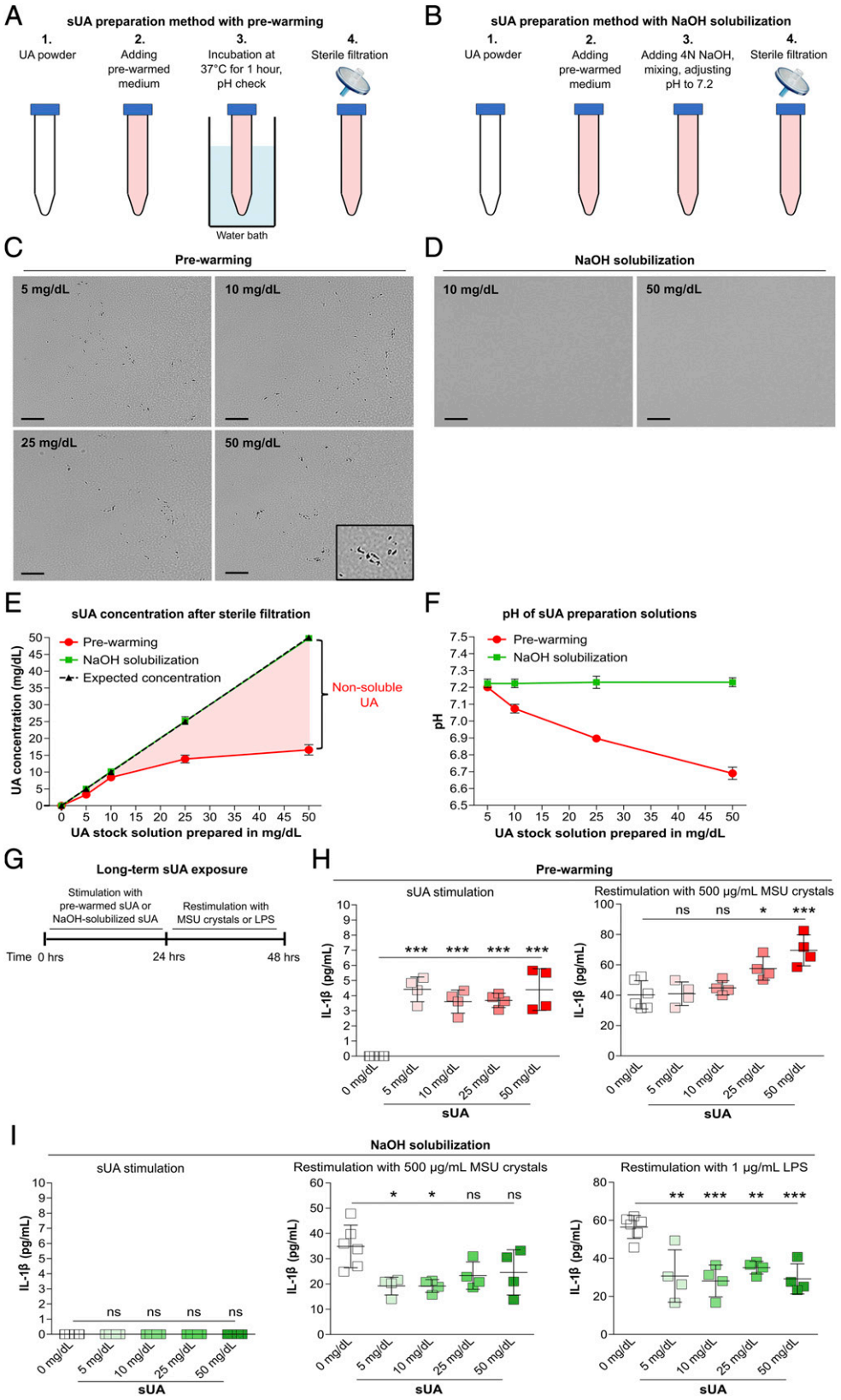

FIGURE 1. UA solubilized with NaOH and long-term exposure inhibits activated monocytes. (**A** and **B**) Workflow of the sUA preparation methods using either prewarmed medium (A) or NaOH solubilization (B) (see *Materials and Methods*). (**C** and **D**) Light microscopy showing UA microcrystals after preparation of prewarmed sUA stock solutions (5–50 mg/dl) (C) but not in the UA stock solutions with NaOH (10 and 50 mg/dl) (D). Original magnification ×400. Scale bar, 10 µm. (**E**) Concentrations of the sUA stock solutions from both UA preparation methods (prewarming and NaOH solubilization) compared with the expected UA concentration determined using an UA assay kit (n = 3 per stock solution). (**F**) pH measurement of sUA stock solutions from both UA preparation methods (prewarming and NaOH solubilization, n = 3 per stock solution). (**G**) Schematic of long-term in vitro stimulation of human THP-1 cells with prewarmed sUA or NaOH-solubilized sUA for 24 h followed by restimulation with MSU crystals or LPS for an additional 24 h. (**H** and **I**) THP-1 cells were incubated with 5–50 mg/dl sUA prepared by prewarming prior to restimulation with 500 µg/ml *(Figure legend continues)*

10% FBS (Biochrom, Berlin, Germany), 2 mM glutamine (Life Technologies, Invitrogen, Grand Island, NY), 1 mM sodium pyruvate, 10 mM HEPES, and 1% penicillin/streptomycin (PAA Laboratories, Pasching, Austria). Cells were incubated at 37˚C in 5% CO_2.

THP-1 cells were cultured in six-well plates (Costar; Corning Incorporated, Corning, NY) at a cell density of 1×10^6 cells per well and preincubated with or without 10 mg/dl sUA for 1 h (short-term exposure) prior to stimulation with 10 μg/ml LPS, 200 μg/ml MSU crystals, or 100 ng/ml human TNF-α for another 4 h. For long-term exposure experiments, UA was prepared with two different preparation methods, and THP-1 cells were stimulated with UA (5–50 mg/dl UA stock solutions) for 24 h and washed with D-PBS, and fresh media were added prior to stimulation with LPS (1 μg/ml) or MSU crystals (500 μg/ml) for 24 h. Cells were harvested for RNA preparation and quantitative RT-PCR (qRT-PCR) (*NFKB-p50*, *NLRP3*, *ASC*, *IL-6*, *TNF-α*), and culture supernatants were collected and stored at −80˚C until analysis. THP-1 cells, $CD14^+$ monocytes, and human primary tubular epithelial cells (40) were quantified for mRNA expression levels of urate transporters via qRT-PCR (human primer sequences are listed in Table II) and for protein quantification of SLC2A9 Western immunoblotting.

Small interfering RNA transfection

SLC2A9 (GLUT9) and control small interfering RNA (siRNAs) (iBONi siRNA pool) were purchased from RIBOXX (Radebeul, Germany). THP-1 cells (1×10^6 cells per well) were transiently transfected with 120 nM control siRNA and SLC2A9 siRNA using Neon transfection system (Thermo Fisher Scientific). The electroporation parameters were as follows: Pulse voltage 700 v, Pulse width 40 ms, and Pulse number 4. RPMI medium was changed with complete RPMI medium (10% FBS, 1% penicillin/streptomycin) after 4 h posttransfection. Forty-eight hours after transfection, THP-1 cells were preincubated with 10 mg/dl sUA for 1 h prior to stimulation with 10 μg/ml LPS or 100 ng/ml TNF-α for another 4 h.

UA uptake assay

Human THP-1 cells (1×10^6 cells per well) were pretreated with or without 10 mg/dl sUA for 1 and 4 h in complete RPMI media and then treated with 10 μg/ml LPS or 100 ng/ml human TNF-α for another 4 h. Culture supernatants were collected, and the cells were harvested, washed with D-PBS, and digested (41). The concentrations of sUA in cell culture supernatants (extracellular) and cytosol (intracellular) were measured by a commercial UA assay kit (BioAssay Systems, Hayward, CA), and the intracellular sUA uptake rates were determined by adjusting UA levels to cell number in each sample.

Analysis of open access gene expression profiles

We analyzed expression patterns of urate reabsorption transporters *SLC2A9*, *SLC22A11*, *SLC22A12*, and *SLC22A13* and urate excretion transporters *SLC2A6*, *ABCC4*, *ABCG2*, *SLC17A1*, and *SLC17A3* as previously described of either PBMCs ($n = 4$ controls) (17), human monocytes ($n = 11$ controls) (42), and human primary tubular epithelial cells ($n = 3$ controls) (43). All data were downloaded as processed expression matrix without quality control, which means that the reliability of the RNA sequencing and the Affymetrix GeneChip microarray is unknown. The formal analysis may deviate from the following results. RNA sequencing of PBMCs (GSE107821: platform Illumina HiSeq 2000–*Homo sapiens*) and human tubular epithelial cells (GSE115960: platform Illumina HiSeq 2500–*Homo sapiens*) used a reads per kilobase per million reads algorithm, and the microarray of monocytes (GSE9988) used the Affymetrix Human Genome U133 Plus 2.0 Array, in which the robust multiarray average algorithm is used, both to normalize and count gene expression. The genes *PTPRC* and *CD14* were used as positive control for PBMCs and monocytes. For primary tubular epithelial cells, we used *PTPRC* and *CD14* as negative controls. Heat maps were generated using the MultiExperiment Viewer (v4.2) software.

Formation and quantification of human neutrophil extracellular traps

For indirect neutrophil extracellular traps that release via soluble mediators, supernatants from activated human $CD14^+$ monocytes (as indicated above) were added to freshly isolated neutrophils (2×10^5 cells per well/200 μl in eight-well microslides; Ibidi, Martinsried, Germany) from healthy individuals for 3 h. Afterwards, neutrophils were fixed with 4% paraformaldehyde and neutrophil extracellular traps stained, as previously described (36). The percent area of citrullinated histone H3 (red; Cell Signaling, Danvers, MA) and neutrophil elastase (green; Santa Cruz Biotechnology, Santa Cruz, CA) was quantified for neutrophil extracellular traps using ImageJ software.

RNA preparation and qRT-PCR

The RNA extraction kit (Qiagen) was used to isolate total RNA from human $CD14^+$ monocytes, primary tubular epithelial cells, and THP-1 cells following manufacturer's instructions. The isolated RNAs were quantified using the Nano drop (PEQLAB Biotechnology GMBH, Erlangen, Germany), and RNA integrity was assessed with 1% agarose gels before being transcribed into cDNA using reverse transcriptase (Superscript II) (Invitrogen). Real-time qRT-PCR was performed using Light Cycler 480 (Roche) with SYBR Green PCR detection dye system (SYBR Green I 96 protocol LC480 Roche running program). All gene expression values were normalized to *GAPDH* as housekeeping gene. All human primers used for amplification were purchased from Metabion and are listed in Table I.

Western immunoblotting

Human THP-1 cells were lysed with radioimmunoprecipitation assay buffer containing phosphatase and protease inhibitor (Roche), and protein concentration was measured (Bio-Rad Protein Assay). Protein samples (30 μg) were mixed with 4× sample loading buffer (Thermo Fisher Scientific), denatured at 95˚C for 5 min, and loaded on Tris/HCl Gel 4–20% (Bio-Rad). Using wet transfer system (Bio-Rad), protein was transferred onto 0.2-μm nitrocellulose blotting membranes (GE Healthcare Life Sciences, Amersham). Membranes were blocked with 5% nonfat dry milk or 5% BSA in TBS-Tween (0.1% Tween 20) for 1 h at room temperature. The following primary human Abs were used: SLC2A9 (0.5 μg/ml, 1 h, room temperature; NOVUS Biologicals, Wiesbaden-Nordenstadt, Germany) and β-actin (1:1000, 1 h, room temperature; Cell Signaling Technology, Frankfurt am Main, Germany). After being washed with TBS-Tween 20, membranes were incubated with secondary Abs: goat anti-mouse (1:2000) or goat anti-rabbit (1:2000) IgG labeled with HRP (1 h, room temperature; both from Cell Signaling Technology). Immunostained bands were detected using a chemiluminescence kit (ECL Kit; Lumigen, Southfield, MI) and the relative protein ratio SLC2A9/β-actin quantified by ImageJ.

ELISA

Concentrations of mouse IL-6 and IL-1β in air pouch extracts were measured using mouse ELISA kits (RayBiotech, Norcross, GA), and human IL-1β in THP-1 supernatants was measured using a human ELISA kit (BioLegend, San Diego, CA) according to manufacturers' protocols. Absorbance was measured on a Multiskan EX reader (Thermo Fisher Scientific, Langenselbold, Germany).

Statistical analysis

Statistical analysis was performed using GraphPad Prism 7 software. Data were compared by Student *t* test to test for significance between two groups, one-way ANOVA with Tukey post hoc test between three or more groups, or by two-way ANOVA with Bonferroni comparison post hoc test when using two parameters with multiple groups. Data are presented as mean ± SD. Differences were considered significant if $p < 0.05$.

Results

sUA preparation containing microcrystals elicits opposite effects in monocytes

Two different sUA preparation methods are mainly reported in the literature: prewarming UA (Fig. 1A) (17, 18, 20, 22, 37, 38) and solubilizing UA with NaOH (Fig. 1B) (39, 44). Checking the prepared solutions for contaminant crystals by light microscopy, we observed microcrystals even after sterile filtration of the UA solutions (5–50 mg/dl) upon prewarming UA but not upon

MSU crystals for 24 h (H) or with 5–50 mg/dl sUA prepared by NaOH solubilization prior to restimulation with 500 μg/ml MSU crystals or 1 μg/ml LPS (l) for 24 h. Supernatants from both preparations were collected for IL-1β ELISA ($n = 4$–6 per group; one-way ANOVA). Data are mean ± SD. *$p < 0.05$, **$p < 0.01$, ***$p < 0.001$ by one-way ANOVA.

Table I. Murine primer sequences

Mouse Genes	Primer Sequences
KIM-1	Forward 5′-TCAGCTCGGGAATGCACAA-3′
	Reverse 5′-TGGTTGCCTTCCGTGTCTCT-3′
Tnfα	Forward 5′-CCACCACGCTCTTCTGTCTAC-3′
	Reverse 5′-AGGGTCTGGGCCATAGAACT-3′
Fibronectin 1	Forward 5′-GGAGTGGCACTGTCAACCTC-3′
	Reverse 5′-ACTGGATGGGGTGGGAAT-3′
18s RNA	Forward 5′-GCAATTATTCCCCATGAACG-3′
	Reverse 5′-AGGGCCTCACTAAACCATCC-3′

Table II. Human primer sequences

Human Genes	Primer Sequences
NLRP3	Forward 5′-CTTCTCTGATGAGGCCCAAG-3′
	Reverse 5′-GCAGCAAACTGGAAAGGAAG-3′
ASC	Forward 5′-AGCTCACCGCTAACGTGCTGC-3′
	Reverse 5′-GCTTGGCTGCCGACTGAGGAG-3′
IL-6	Forward 5′-ACAAATTCGGTACATCCTC-3′
	Reverse 5′-GCAGAATGAGATGAGTTGT-3′
TNF-α	Forward 5′-CTTCTCCTTCCTGATCGTGG-3′
	Reverse 5′-GCTGGTTATCTCTCAGCTCCA-3′
NFKB-p50	Forward 5′-GCAGCACTACTTCTTGACCACC-3′
	Reverse 5′-TCTGCTCCTGAGCATTGACGTC-3′
IL-12p40	Forward 5′-GACATTCTGCGTTCAGGTCCAG-3′
	Reverse 5′-CATTTTTGCGGCAGATGACCGTG-3′
IL-10	Forward 5′-CTGTGAAAACAAGAGCAAGGC-3′
	Reverse 5′-GAAGCTTCTGTTGGCTCCC-3′
SLC2A9	Forward 5′-GCTCTTGGAGAAGCACAACGAG-3′
	Reverse 5′-ACACCAGGCGGATGCTCCTCT-3′
SLC22A12	Forward 5′-TTGATTGGCAGGAGGTGACC-3′
	Reverse 5′-GGTTAAGTGGAGTCGGTCAG-3′
SLC22A6	Forward 5′-CCACCTCTTCCTCTGCCTCTCCAT-3′
	Reverse 5′-GTCTGTTTCCCTTTCCTGCTCTCC-3′
SLC22A11	Forward 5′-CAGACCAAGCACTTCAGGAGCT-3′
	Reverse 5′-TCCTTCACGCTGGACATCAGCA-3′
SLC22A13	Forward 5′-TTTCCGCAACTGGAGGCTCCTT-3′
	Reverse 5′-GTTGTATCGCCTCGTCCATCCT-3′
ABCC4	Forward 5′-CTGTTGGAGGATGGTGATCTGAC-3′
	Reverse 5′-CTGCTAACTTCCGCATCTACTGC-3′
ABCG2	Forward 5′-GTTCTCAGCAGCTCTTCGGCTT-3′
	Reverse 5′-TCCTCCAGACACACCACGGATA-3′
SLC17A1	Forward 5′-GCACAGATCCACATGGTTTGCC-3′
	Reverse 5′-CACCATAGGAGGTGGAACTCAAG-3′
SLC17A3	Forward 5′-GCCTGTTGACTCATTTGGTGGC-3′
	Reverse 5′-GGAGCCATTGTCAGTATGCCAC-3′
GAPDH	Forward 5′-GTCTCCTCTGACTTCAACAGCG-3′
	Reverse 5′-ACCACCCTGTTGCTGTAGCCAA-3′

solubilizing UA with NaOH (Fig. 1C, 1D). Indeed, the final sUA concentration in the prewarming preparation containing microcrystals was much lower than predicted from the input of UA substrate (only 30% at the highest concentration), whereas the final sUA concentration upon NaOH-based sUA preparation exactly matched the UA substrate input (Fig. 1E). Obviously, prewarming solubilized only a part of the UA substrate, whereas the other part got or remained incorporated in UA crystals contaminating the final sUA preparation. We observed a pH drop in the prewarmed solutions, whereas the crystal-free NaOH-based sUA preparation solutions were stable at the adjusted pH of 7.2 (Fig. 1F). Next, we tested both preparations on the inflammatory function in THP-1 cells incubated with either sUA preparation for 24 h prior to restimulation with MSU crystals or LPS (Fig. 1G, long-term sUA exposure). Whereas prewarmed sUA alone triggered the release of IL-1β and augmented this response upon subsequent MSU crystal exposure (Fig. 1H), NaOH-solubilized sUA did not induce IL-1β release and showed only a minor effect upon MSU crystal challenge (Fig. 1I). These data indicate that the proinflammatory effects of sUA prepared by prewarming do not relate to sUA per se but to microcrystal contaminants creating erroneous results and misinterpretations. In contrast, NaOH solubilization generates a crystal-free sUA preparation, which allows studying the true biological effects of sUA.

HU attenuates MSU crystal–induced tissue inflammation

Previously employed rodent models of HU have serious limitations, for example, they do not reach serum concentrations of UA relevant to human disease (17, 20, 21, 23, 26, 45–48). We used a transgenic mouse model based on the selective deactivation of GLUT9 in hepatocytes, which has been reported to develop clinically relevant levels of asymptomatic HU (32, 49). To test for an inhibitory effect of HU during acute tissue inflammation in vivo, we first injected Alb-creERT2;*Glut9*$^{lox/lox}$ and *Glut9*$^{lox/lox}$ control mice with tamoxifen to activate the transgene and placed both groups on a chow diet enriched with the urate precursor inosine (Fig. 2A). Alb-creERT2;*Glut9*$^{lox/lox}$ mice fed an inosine-rich diet developed HU with a serum UA range of 8–12 mg/dl, whereas UA levels remained low in *Glut9*$^{lox/lox}$ mice (healthy) (Fig. 2B). No effect on kidney function was observed between both groups as indicated by similar serum blood urea nitrogen and creatinine levels (Fig. 2C), periodic acid–Schiff staining, and intrarenal mRNA expression levels of *KIM-1*, *Tnfα*, and *Fibronectin 1* (Table I, Supplemental Fig. 1A, 1B), that is, asymptomatic HU.

To mimic acute tissue inflammation as in gouty arthritis, we injected MSU crystals (or vehicle) into dorsal s.c. air pouches in HU and healthy mice (Fig. 2A, 2D). Twelve hours later, air pouch lavage fluids were collected, and flow cytometric analysis of the infiltrating immune cells was performed (Fig. 2E, gating strategy). The number of infiltrating CD45$^+$ leukocytes and CD45$^+$Ly6G–Ly6C$^+$ monocytes in control mice injected with MSU crystals significantly increased compared with vehicle-treated mice (Fig. 2F, 2G). However, mice with HU displayed significantly fewer CD45$^+$ cells and monocytes (Fig. 2F, 2G) as well as neutrophils (healthy: 18,756 ± 2011 and HU: 14,319 ± 1480, data not shown) in MSU crystal–injected pouch fluids. Pouch fluid levels of IL-1β and IL-6 were reduced in mice with HU accordingly (Fig. 2H, 2I). Taken together, the data show that HU attenuates MSU crystal–induced tissue inflammation by suppressing leukocyte recruitment and activation.

HU suppresses the activation of human CD14$^+$ monocytes

To test whether NaOH-solubilized sUA exerts inhibitory effects also in human monocytes after short-term sUA exposure, we isolated CD14$^+$ monocytes from the blood of healthy subjects (Fig. 3A) and preincubated the cells with 10 mg/dl sUA prior to stimulation with LPS, MSU crystals, or medium alone (Fig. 3B, short-term exposure). Upon MSU crystal or LPS stimulation, the mRNA expression levels of *NLRP3*, *TNF-α*, and *IL-6* significantly increased compared with medium (Fig. 3C). However, the presence of sUA suppressed mRNA expression levels of *NLRP3*, *IL-6*, and *TNF-α* in CD14$^+$ monocytes stimulated with LPS or MSU crystals (Fig. 3C, Table II). Flow cytometric analysis for the intracellular cytokines IL-6 and TNF-α confirmed that sUA significantly reduced the number of IL-6 and TNF-α single-positive as well as of IL-6/TNF-α double-positive CD14$^+$ monocytes compared with LPS or MSU crystal stimulation only (Fig. 3D).

To confirm a suppressive effect of sUA on monocytes also in patients, we treated CD14$^+$ blood monocytes isolated from hyperuricemic CKD patients as well as healthy subjects with MSU crystals, LPS, or medium alone for 4 h. Upon stimulation with MSU crystals, the mRNA expression levels of *NLRP3*, *ASC*, *IL-6*,

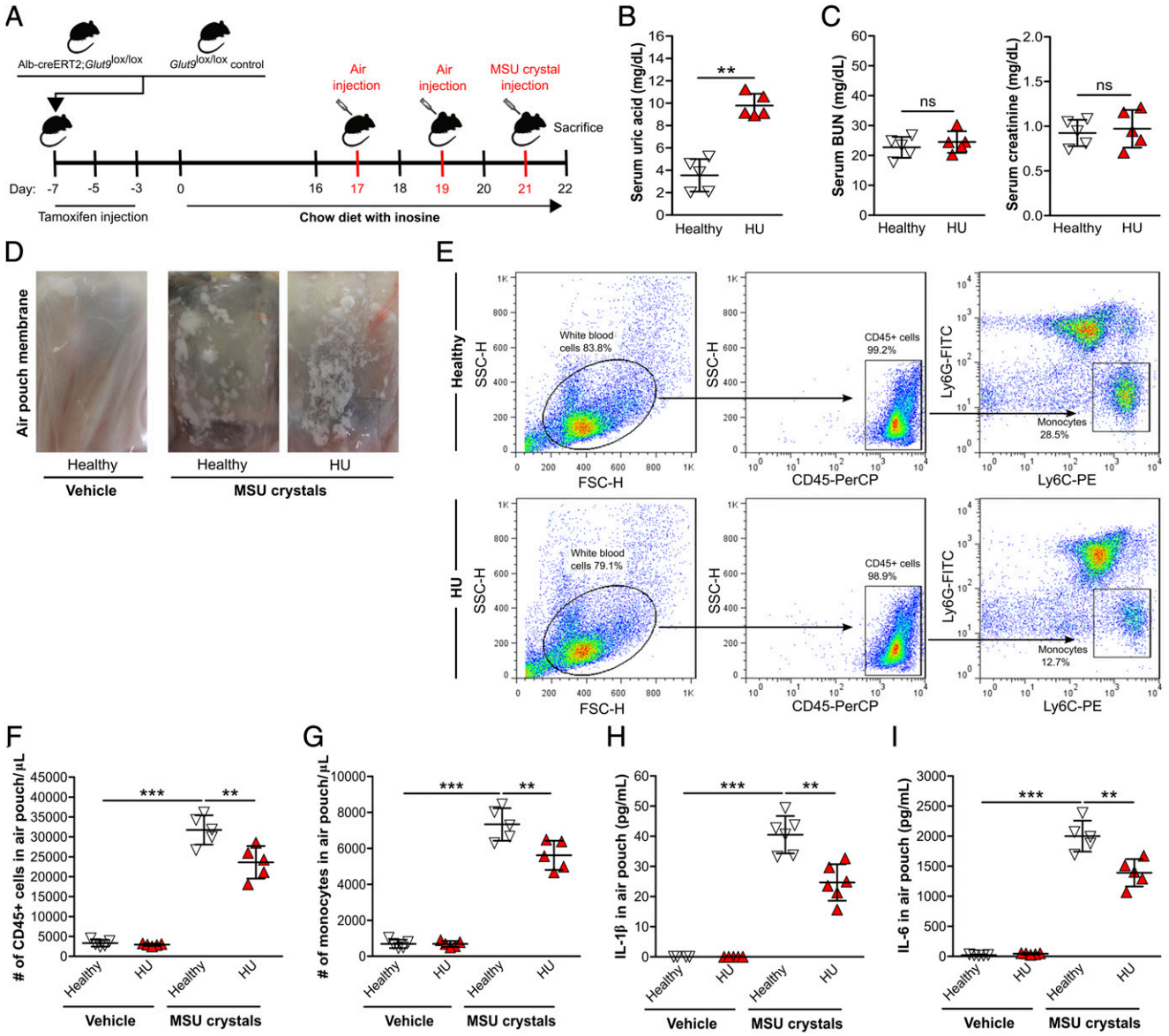

FIGURE 2. Leukocyte recruitment is reduced in MSU crystal–induced tissue inflammation in mice with HU. (**A**) Experimental design of the HU and MSU crystal–induced tissue inflammation animal model. Alb-creERT2;*Glut9*$^{lox/lox}$ mice and *Glut9*$^{lox/lox}$ control mice were injected i.p. with tamoxifen. Both groups were fed a standard chow diet enriched with inosine for 22 d. On day 21, mice received an s.c. injection of MSU crystals or vehicle into a preexisting air pouch and were sacrificed 12 h later. (**B** and **C**) Serum UA (B), blood urea nitrogen (BUN), and creatinine (C) levels of *Glut9*$^{lox/lox}$ mice with chow diet and inosine (healthy) and Alb-creERT2;*Glut9*$^{lox/lox}$ mice with chow diet and inosine (HU) on day 22 ($n = 5$ mice per group; Student t test). (**D**) Representative images of air pouch membranes of vehicle and MSU crystal–injected air pouches. (**E**) Flow cytometric analysis illustrating infiltrating CD45$^+$ cells and CD45$^+$Ly6G$^-$Ly6C$^+$ monocytes in MSU crystal–injected air pouches from healthy and HU mice. (**F** and **G**) Absolute numbers of CD45$^+$ cells (F) and monocytes (G) in air pouch per microliter from mice with or without MSU crystals determined by flow cytometry ($n = 5$ mice per group). (**H** and **I**) Concentrations of IL-1β (H) and IL-6 (I) measured in the air pouch fluid via ELISA ($n = 5$ mice per group). Data are mean ± SD. $^{**}p < 0.01$, $^{***}p < 0.001$ by two-way ANOVA.

NF-κB, *IL-6*, *TNF-α*, and *IL-12p40* increased in CD14$^+$ monocytes from healthy individuals compared with untreated monocytes (medium) (Fig. 3E). However, this strong inflammatory response of MSU crystal–activated CD14$^+$ monocytes from healthy individuals (healthy) was significantly inhibited in activated CD14$^+$ monocytes from hyperuricemic patients (HU), except for the anti-inflammatory cytokine IL-10, which increased in mRNA expression (Fig. 3E). LPS stimulation gave similar results, wherein all of the tested genes were significantly downregulated in monocytes from HU patients (Fig. 3F). To test whether sUA in the plasma from HU patients contributes to the intrinsic dysfunction of monocytes from HU patients versus healthy controls, we isolated CD14$^+$ monocytes from healthy subjects and preincubated the cells with plasma from either HU patients or healthy individuals. The plasma contained UA levels as follows: HU was 9.73 ± 0.50 mg/dl, and healthy was 4.17 ± 0.46 mg/dl. HU plasma decreased the inflammatory function of LPS-activated CD14$^+$ monocytes from healthy donors compared with activated CD14$^+$ monocytes that were incubated with plasma from healthy subjects, an effect entirely reversed by pretreating plasma with rasburicase (Fig. 3G).

As macrophage-derived soluble mediators, including IL-1β and TNF-α, can promote neutrophil extracellular trap release (50), we also tested the effect of supernatants from MSU crystal– or LPS-activated CD14$^+$ monocytes on freshly isolated neutrophils from healthy subjects. Indeed, soluble mediators released from LPS- or

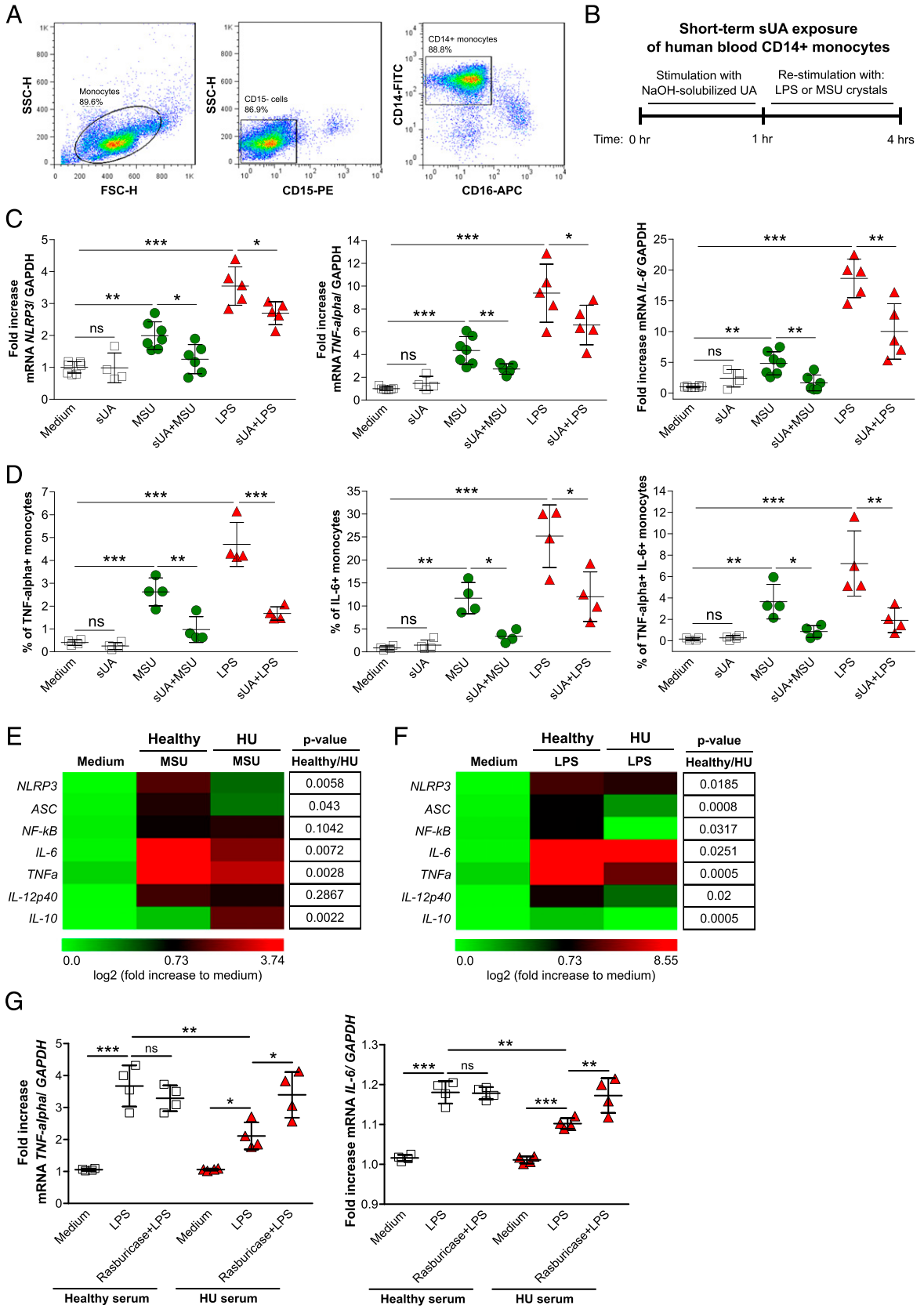

FIGURE 3. sUA inhibits the inflammatory function of human CD14$^+$ monocytes. (**A**) Human blood CD14$^+$ monocytes were isolated from healthy individuals (see *Materials and Methods*) and identified as CD15$^-$CD16$^-$CD14$^+$ by flow cytometry (with gating strategy) with a purity of ∼88%. (**B**) Schematic of short-term in vitro stimulation of human CD14$^+$ monocytes with NaOH-solubilized sUA for 1 h followed by restimulation with MSU crystals or LPS for an additional 4 h. (**C**) CD14$^+$ monocytes were preincubated with 10 mg/dl sUA (short-term sUA exposure) prior to stimulation with MSU crystals or LPS or left untreated (medium). After stimulation, RNA expression levels of the genes *NLRP3*, *TNF-α*, and *IL-6* were determined via RT-PCR (n = 4–7 per group; one-way ANOVA). (**D**) CD14$^+$ monocytes were short-term preincubated with 10 mg/dl sUA and then stimulated with MSU crystals or LPS or left untreated (medium) for 8 h. After stimulation, the percentage of TNF-α$^+$IL-6$^-$, TNF-α$^-$IL-6$^+$, and TNF-α$^+$IL-6$^+$ *(Figure legend continues)*

MSU crystal–activated $CD14^+$ monocytes induced neutrophil extracellular trap release (Supplemental Fig. 2). This effect was attenuated by supernatants from sUA + MSU crystals with a significant effect from sUA + LPS-stimulated monocytes (Supplemental Fig. 2). The data indicate that short-term exposure with NaOH-solubilized sUA inhibits the inflammatory effects of activated $CD14^+$ monocytes, an effect that was confirmed in $CD14^+$ monocytes from HU patients.

sUA modulates monocyte function by intracellular uptake via the urate transporter SLC2A9

How could sUA inhibit the inflammatory function of human monocytes? As a receptor-mediated outside-in signaling mechanism seemed less likely, we speculated on a urate transporter-mediated uptake of sUA inside the cells. However, there is a paucity of data on the expression of urate transporters in immune cells; hence, we first sought to identify urate transporters expressed by monocytes. RNA-sequencing data of PBMCs and human primary tubular epithelial cells from the public domain (17, 43) and microarray data of human monocytes (42) suggested that these cells selectively express the urate reabsorption transporter SLC2A9, whereas primary tubular epithelial cells express all known urate transporters (Fig. 4A). RT-PCR of various other urate transporters confirmed the selective expression of SLC2A9 in human $CD14^+$ monocytes and THP-1 cells, whereas primary tubular epithelial cells, used as positive control, expressed most of them (Fig. 4B, 4C, Table II).

If SLC2A9 is involved in the immunomodulatory effects of sUA on monocytes, it should mediate the intracellular uptake of sUA. Indeed, exposing LPS-activated THP-1 cells to 10 mg/dl sUA for 1 and 4 h resulted in an increase of intracellular sUA concentration (Fig. 4D, 4E).

Next, we preincubated THP-1 cells with or without 10 mg/dl sUA for 1 h (short-term) prior to stimulation with LPS for 4 h and found that the presence of LPS significantly reduced extracellular sUA levels and increased intracellular levels of sUA in UA-treated THP-1 cells (Fig. 4F–H). Benzbromarone, an inhibitor of several urate transporters, attenuated the LPS-induced intracellular uptake of sUA (Fig. 4H). LPS stimulation did not affect the mRNA and protein expression level of *SLC2A9* (Fig. 4I, 4J). Despite the fact that LPS activation did not alter the expression of *SLC2A9* in sUA-treated THP-1 cells, we observed a significant decrease in the mRNA expression of the inflammatory genes *NFKB-p50*, *ASC*, *NLRP3*, *IL-6*, and *TNF-α* when LPS- or human TNF-α–activated THP-1 cells were preincubated with 10 mg/dl sUA (Fig. 4K, Supplemental Fig. 3A).

To test for a role of SLC2A9 in this context, we silenced SLC2A9 by specific siRNA in THP-1 cells as confirmed by RT-PCR and immunoblotting (Fig. 5A–C). SLC2A9 silencing significantly attenuated the suppressive effect of LPS on extracellular and intracellular sUA levels, which implies that SLC2A9 mediates sUA uptake into activated monocytes (Fig. 5D, 5E). As a consequence, SLC2A9 silencing abolished the suppressive effect of sUA on the mRNA expression of *NFKB-p50*, *IL-6*, and *TNF-α* (Fig. 5F). The same effect of sUA uptake on the inflammatory function in THP-1 cells was observed in response to TNF-α upon silencing the SLC2A9 urate transporter (Supplemental Fig. 3B–E). We conclude that SLC2A9-mediated intracellular uptake of sUA is an essential step in UA-related suppression of activated monocytes in response to inflammatory stimuli.

Discussion

We had hypothesized that the discrepant literature on the immune effects of sUA may relate to how sUA is actually prepared and that only a microcrystal-free sUA preparation will give reliable results. Indeed, our in vitro studies clearly identify that sUA prepared by prewarming produces erroneous proinflammatory results for a contamination with UA microcrystals. A proper crystal-free preparation reveals anti-inflammatory effects of sUA on activated monocytes, driven by SLC2A9-mediated intracellular uptake of sUA. The suppressed inflammatory immune response of sUA was confirmed in $CD14^+$ monocytes from hyperuricemic patients. As our in vivo experiments in a meaningful model of asymptomatic HU and MSU crystal–induced tissue inflammation validate this finding, we conclude that sUA is an intrinsic inhibitor of tissue inflammation also if triggered by MSU crystals.

Several in vitro studies reported proinflammatory effects of sUA using another protocol for sUA preparation that (17, 18, 20, 22, 38, 51–55), as we show in this article, contains crystalline particles that are well-known activators of sterile inflammation (56). Therefore, such effects cannot be attributed to sUA. Previous in vitro studies reported that NaOH-solubilized sUA does not elicit an inflammatory response by immune cells (39, 44) and that sUA can act as a potent scavenger of singlet oxygen (57, 58) and inhibitor of UMP synthase to antagonize the cytotoxic effects of the chemotherapeutic agent 5-fluorouracil (59). The solubility of UA strongly depends on the preparation solution and the physiological pH range. UA can be solubilized in NaOH as recommended by commercial suppliers, such as Sigma-Aldrich, but not simply in D-PBS or prewarmed cell culture medium. In a previous study, Iwata et al. (60) found that the solubility of UA increases with the rise in pH and that long-term incubation at 37˚C can decrease the total dissolved UA concentration due to crystallization. This would indicate that besides the pH range (7.0–7.4), the concentration and storage time of the stock solution can influence the solubility of UA, which should be considered when performing in vitro experiments. The mechanism of crystallization, nucleation, and crystal growth involves a combination of critical processes, including concentration of solutes, temperature, and pH. For example, crystallization of calcium oxalate crystals strongly depends on the pH (61), which is associated with kidney diseases (62, 63) because of a decline in urinary pH. Similar physiochemical processes apply to MSU and UA crystallization in gouty arthritis (64–66) and UA kidney stone disease (65, 67–69), respectively. Unlike the microcrystal-contaminated prewarmed sUA solution, a crystal-free preparation of sUA rather suppresses

monocytes was determined by intracellular staining using flow cytometry (n = 4 per group). (**E** and **F**) $CD14^+$ monocytes were isolated from healthy individuals (healthy, n = 8) or hyperuricemic CKD patients (HU, n = 10) and stimulated with MSU crystals or LPS or left untreated (medium). After stimulation, RNA expression levels of the genes *NLRP3*, *ASC*, *NF-κB*, *IL-6*, *TNF-α*, *IL-12p40*, and *IL-10* were determined via RT-PCR. Heat maps of gene expression data after MSU crystal (E) and LPS (F) stimulation. Color intensity represents the mean log2 fold change within each row (mean expression value of healthy versus HU). The p values of gene expression differences were calculated between healthy versus HU of stimulated monocytes (Student t test). (**G**) Healthy $CD14^+$ monocytes were incubated with plasma from healthy individuals or hyperuricemic CKD patients (HU) in the absence or presence of rasburicase prior to stimulation with LPS. After stimulation, RNA expression levels of the genes *TNF-α* and *IL-6* were determined via RT-PCR (n = 4 per group; two-way ANOVA). Data are mean ± SD. *$p < 0.05$, **$p < 0.01$, ***$p < 0.001$ by one-way ANOVA.

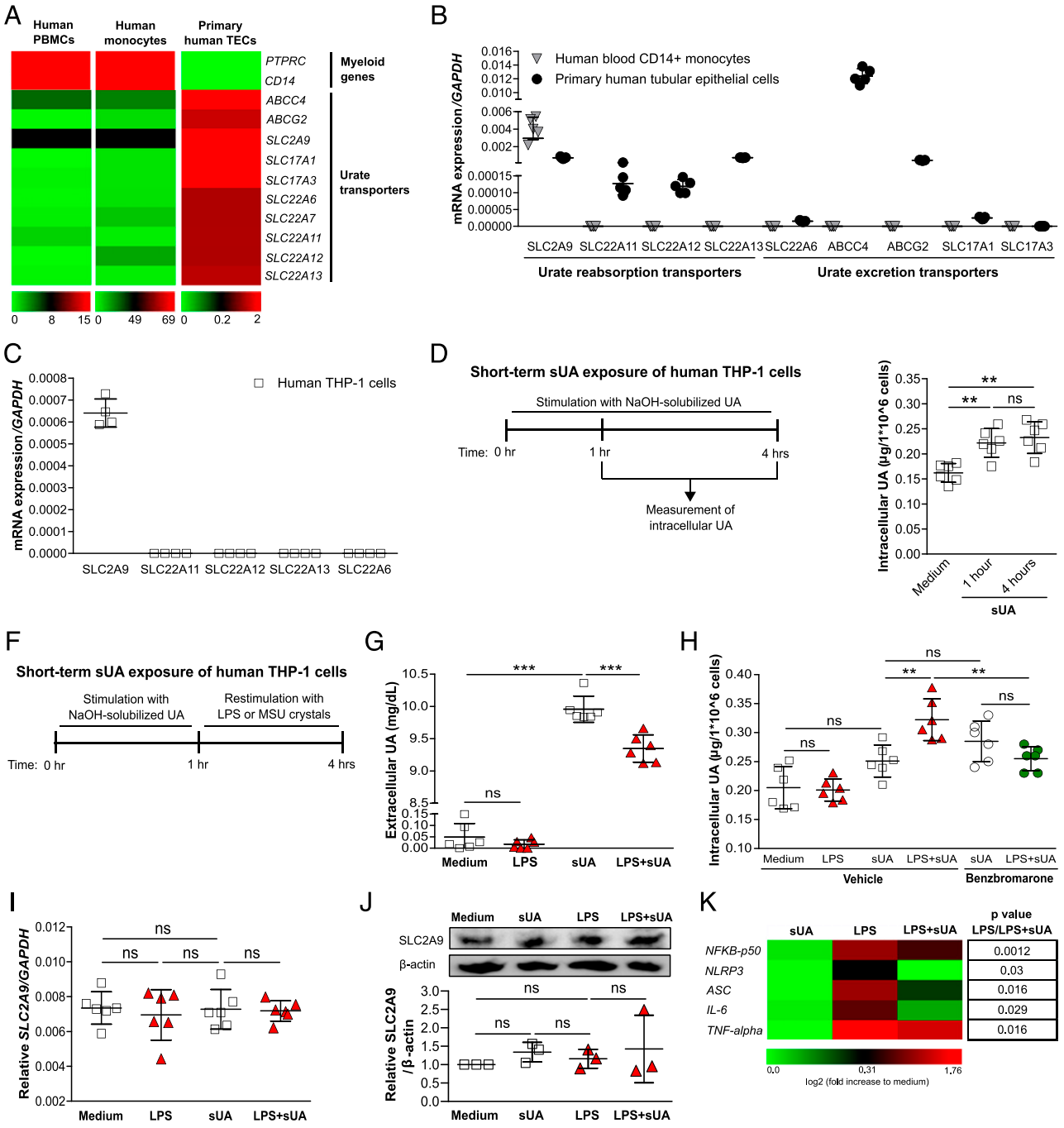

FIGURE 4. sUA modulates LPS-activated monocytes by intracellular uptake via SLC2A9/GLUT9. (**A**) Online available RNA-sequencing data of human blood PBMCs ($n = 4$) and primary human tubular epithelial cells (TECs) (17, 43) and Affymetrix human microarray data of human blood monocytes ($n = 11$) (42), all cell populations are from healthy controls. (**B**) mRNA expression of the UA reabsorption transporters *SLC2A9*, *SLC22A11*, *SLC22A12*, and *SLC22A13* and the UA excretion transporters *SLC22A6*, *ABCC4*, *ABCG2*, *SLC17A1*, and *SLC17A3* in human $CD14^+$ blood monocytes and primary human TECs determined via RT-PCR ($n = 3$–5 per group). (**C**) mRNA expression of the urate transporters *SLC2A9*, *SLC22A11*, *SLC22A12*, *SLC22A13*, and *SLC22A6* in human THP-1 cells determined via RT-PCR ($n = 4$ per group). (**D** and **E**) LPS-activated THP-1 cells were incubated with 10 mg/dl sUA for 1 and 4 h (D), and intracellular sUA levels determined using an UA assay kit (E) ($n = 5$–6 per group; one-way ANOVA). (**F** and **G**) Human THP-1 cells were preincubated with 10 mg/dl NaOH-solubilized sUA for 1 h prior to restimulation with LPS or left untreated (medium) for 4 h (F) (short-term exposure). Culture supernatants were collected, and the concentrations of extracellular sUA were measured (G) ($n = 6$ per group; one-way ANOVA). (**H**) LPS-activated THP-1 cells with or without 10 mg/dl sUA were digested after treatment with vehicle or benzbromarone, and the intracellular sUA concentration was measured ($n = 6$ per group; two-way ANOVA). (**I** and **J**) mRNA ($n = 6$) (I) and protein (J) expression and quantification ($n = 3$) of SLC2A9 from LPS-activated THP-1 cells in the presence or absence of 10 mg/dl sUA were determined by RT-PCR and Western blot (one-way ANOVA). (**K**) After LPS stimulation, mRNA expression levels of *NFKB-p50*, *NLRP3*, *ASC*, *IL-6*, and *TNF-α* were determined via RT-PCR and illustrated as heat map ($n = 6$ per group). Data are mean ± SD. $^{**}p < 0.01$, $^{***}p < 0.001$.

inflammatory responses. Our numerous in vitro experiments were consistent in this regard and were confirmed in $CD14^+$ monocytes isolated from hyperuricemic patients.

The suppressive effect of sUA on the inflammatory function of activated human monocytes may occur following uptake of sUA via urate transporters (8). Although many of the urate transporters are

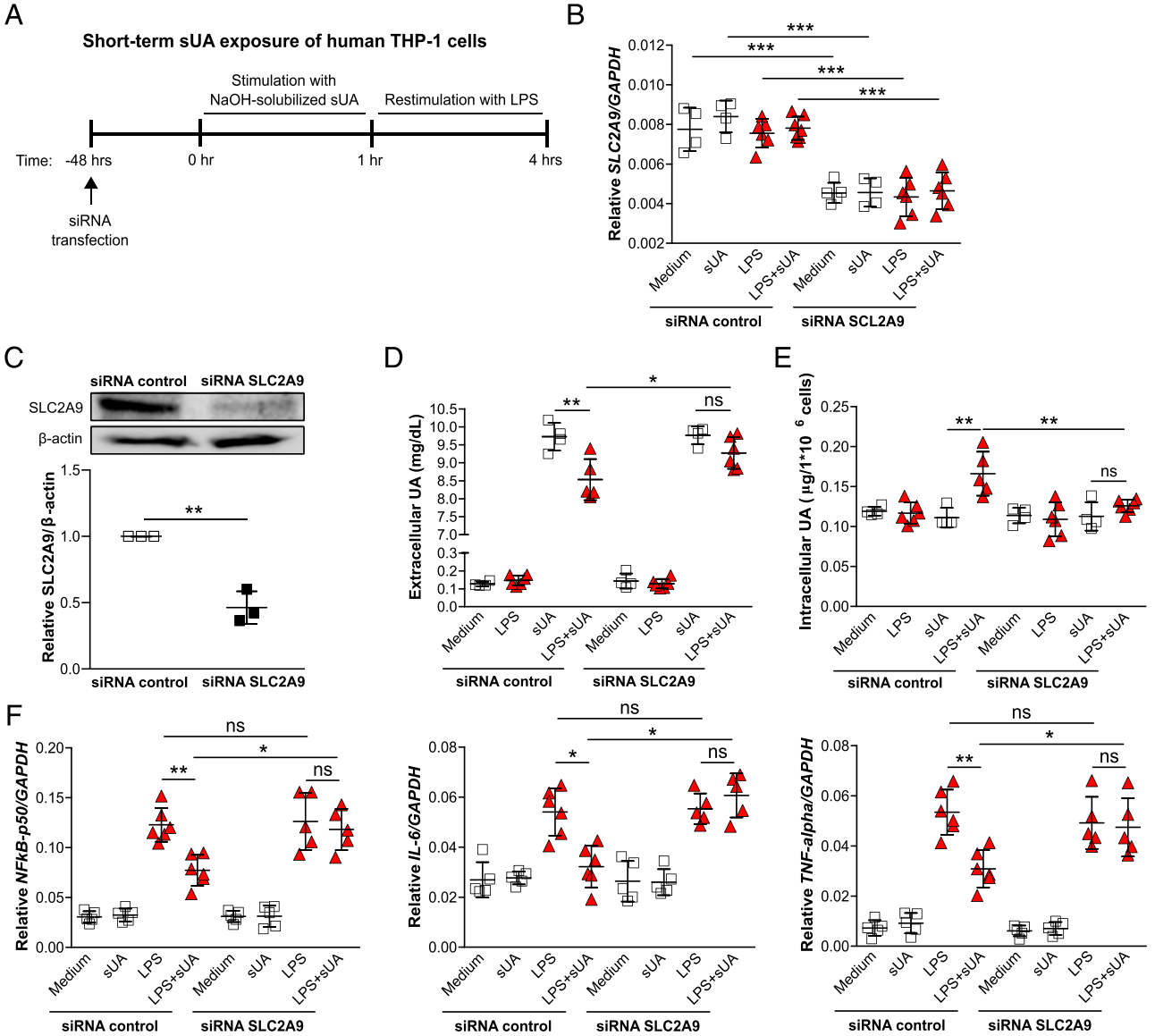

FIGURE 5. Monocytes require activation signals for SLC2A9-mediated uptake of sUA. (**A**) Schematic of SLC2A9 knockdown experiments using specific siRNA (siRNA SLC2A9) or scrambled siRNA (siRNA control) in sUA-incubated LPS-activated human THP-1 cells. (**B**) After transfection and stimulation, relative mRNA expression levels of SLC2A9 were determined via RT-PCR (n = 4–6 per group; two-way ANOVA). (**C**) Protein expression of SLC2A9-unstimulated THP-1 cells after transfection with specific siRNA (siRNA SLC2A9) or scrambled siRNA (siRNA control) and quantification (n = 3, Student t test). (**D**–**F**) Concentration of extracellular sUA (D) and intracellular sUA levels (E) was determined using an UA assay kit (n = 4–6 per group; two-way ANOVA). (F) After transfection and LPS stimulation, relative mRNA expression levels of *NFKB-p50*, *IL-6*, and *TNF-α* were determined by RT-PCR (n = 5–6 per group; two-way ANOVA). Data are mean ± SD. $^*p < 0.05$, $^{**}p < 0.01$, $^{***}p < 0.001$.

highly expressed in the kidney and intestine, recent studies found SLC22A12 and SLC2A9 to be expressed in human endothelial cells, leukocytes, and chondrocytes (37, 70, 71). The urate transporters SLC2A9 (37) and BCRP/ABCG2 (29) can regulate the sUA uptake in human umbilical vascular endothelial cells, which further triggers cell injury and inflammation. Unlike endothelial (37), pancreatic β (72), and vascular smooth muscle (26) cells, we found that the intracellular sUA uptake by human monocytes occurs via SLC2A9 leading to this suppressed phenotype. Whether other transporters apply to other cell types, for example, urate transporters or selective organic anion channels (73), remains to be investigated in future studies.

The overall functional importance of HU in vivo remains controversial because of the lack of a suitable animal model (17, 20, 21, 26). All studies investigating the effect of HU in vivo are based either on i.p. injections of high concentrations of UA (47, 48), oral administration of potassium oxonate (23, 45, 46), unilateral ureter obstruction-induced nephropathy (20), or diabetic nephropathy (21) inducing only very low serum UA levels, which would not even be considered clinically as HU. We have now established an animal model of HU (serum UA levels of ∼10 mg/dl) without kidney impairment that mimics the range of asymptomatic HU in humans more accurately. Using this in vivo approach, we show for the first time, to our knowledge, that HU directly impairs leukocyte recruitment, which diminished MSU crystal–related tissue inflammation.

In conclusion, we identify sUA as an intrinsic inhibitor of innate immunity, a mechanism associated with the intracellular uptake of sUA via SLC2A9 by activated monocytes resulting in a suppressed phenotype. This immunomodulatory property of sUA may explain several clinical observations. First, HU is a relatively common metabolic condition, yet only a minority of patients with HU

(10–15%) develop symptomatic gout (74). Second, a sudden reduction of HU with urate-lowering therapy can elicit acute gout attacks (75), probably because of a sudden decline in the negative regulator of sterile inflammation sUA. In addition, 15% or more individuals with asymptomatic HU have crystal deposits without experiencing classical symptoms (76). Fourth, despite persistent HU, not all patients with chronic kidney disease suffer from acute gout attacks (77). Further studies are needed to better understand the role of asymptomatic HU in gouty arthritis and beyond. It is important to recognize that soluble and crystalline UA have opposite effects in innate immunity.

Acknowledgments

We thank all healthy volunteers involved in this study.

Disclosures

The authors have no financial conflicts of interest.

References

1. Oda, M., Y. Satta, O. Takenaka, and N. Takahata. 2002. Loss of urate oxidase activity in hominoids and its evolutionary implications. *Mol. Biol. Evol.* 19: 640–653.
2. Kratzer, J. T., M. A. Lanaspa, M. N. Murphy, C. Cicerchi, C. L. Graves, P. A. Tipton, E. A. Ortlund, R. J. Johnson, and E. A. Gaucher. 2014. Evolutionary history and metabolic insights of ancient mammalian uricases. *Proc. Natl. Acad. Sci. USA* 111: 3763–3768.
3. Enomoto, A., H. Kimura, A. Chairoungdua, Y. Shigeta, P. Jutabha, S. H. Cha, M. Hosoyamada, M. Takeda, T. Sekine, T. Igarashi, et al. 2002. Molecular identification of a renal urate anion exchanger that regulates blood urate levels. *Nature* 417: 447–452.
4. Köttgen, A., E. Albrecht, A. Teumer, V. Vitart, J. Krumsiek, C. Hundertmark, G. Pistis, D. Ruggiero, C. M. O'Seaghdha, T. Haller, et al; MAGIC Consortium. 2013. Genome-wide association analyses identify 18 new loci associated with serum urate concentrations. *Nat. Genet.* 45: 145–154.
5. Vitart, V., I. Rudan, C. Hayward, N. K. Gray, J. Floyd, C. N. Palmer, S. A. Knott, I. Kolcic, O. Polasek, J. Graessler, et al. 2008. SLC2A9 is a newly identified urate transporter influencing serum urate concentration, urate excretion and gout. *Nat. Genet.* 40: 437–442.
6. Matsuo, H., T. Takada, K. Ichida, T. Nakamura, A. Nakayama, Y. Ikebuchi, K. Ito, Y. Kusanagi, T. Chiba, S. Tadokoro, et al. 2009. Common defects of ABCG2, a high-capacity urate exporter, cause gout: a function-based genetic analysis in a Japanese population. *Sci. Transl. Med.* 1: 5ra11.
7. Enomoto, A., and H. Endou. 2005. Roles of organic anion transporters (OATs) and a urate transporter (URAT1) in the pathophysiology of human disease. *Clin. Exp. Nephrol.* 9: 195–205.
8. So, A., and B. Thorens. 2010. Uric acid transport and disease. *J. Clin. Invest.* 120: 1791–1799.
9. Lawrence, R. C., D. T. Felson, C. G. Helmick, L. M. Arnold, H. Choi, R. A. Deyo, S. Gabriel, R. Hirsch, M. C. Hochberg, G. G. Hunder, et al; National Arthritis Data Workgroup. 2008. Estimates of the prevalence of arthritis and other rheumatic conditions in the United States. Part II. *Arthritis Rheum.* 58: 26–35.
10. Neogi, T. 2011. Clinical practice. Gout. *N. Engl. J. Med.* 364: 443–452.
11. Nishimura, A., T. Akahoshi, M. Takahashi, K. Takagishi, M. Itoman, H. Kondo, Y. Takahashi, K. Yokoi, N. Mukaida, and K. Matsushima. 1997. Attenuation of monosodium urate crystal-induced arthritis in rabbits by a neutralizing antibody against interleukin-8. *J. Leukoc. Biol.* 62: 444–449.
12. Guerne, P. A., R. Terkeltaub, B. Zuraw, and M. Lotz. 1989. Inflammatory microcrystals stimulate interleukin-6 production and secretion by human monocytes and synoviocytes. *Arthritis Rheum.* 32: 1443–1452.
13. Tramontini, N., C. Huber, R. Liu-Bryan, R. A. Terkeltaub, and K. S. Kilgore. 2004. Central role of complement membrane attack complex in monosodium urate crystal-induced neutrophilic rabbit knee synovitis. *Arthritis Rheum.* 50: 2633–2639.
14. Di Giovine, F. S., S. E. Malawista, G. Nuki, and G. W. Duff. 1987. Interleukin 1 (IL 1) as a mediator of crystal arthritis. Stimulation of T cell and synovial fibroblast mitogenesis by urate crystal-induced IL 1. *J. Immunol.* 138: 3213–3218.
15. Hahn, J., J. Knopf, C. Maueröder, D. Kienhöfer, M. Leppkes, and M. Herrmann. 2016. Neutrophils and neutrophil extracellular traps orchestrate initiation and resolution of inflammation. *Clin. Exp. Rheumatol.* 34(4 Suppl. 98): 6–8.
16. di Giovine, F. S., S. E. Malawista, E. Thornton, and G. W. Duff. 1991. Urate crystals stimulate production of tumor necrosis factor alpha from human blood monocytes and synovial cells. Cytokine mRNA and protein kinetics, and cellular distribution. *J. Clin. Invest.* 87: 1375–1381.
17. Crişan, T. O., M. C. P. Cleophas, B. Novakovic, K. Erler, F. L. van de Veerdonk, H. G. Stunnenberg, M. G. Netea, C. A. Dinarello, and L. A. B. Joosten. 2017. Uric acid priming in human monocytes is driven by the AKT-PRAS40 autophagy pathway. *Proc. Natl. Acad. Sci. USA* 114: 5485–5490.
18. Crişan, T. O., M. C. Cleophas, M. Oosting, H. Lemmers, H. Toenhake-Dijkstra, M. G. Netea, T. L. Jansen, and L. A. Joosten. 2016. Soluble uric acid primes TLR-induced proinflammatory cytokine production by human primary cells via inhibition of IL-1Ra. *Ann. Rheum. Dis.* 75: 755–762.
19. Mylona, E. E., M. Mouktaroudi, T. O. Crisan, S. Makri, A. Pistiki, M. Georgitsi, A. Savva, M. G. Netea, J. W. van der Meer, E. J. Giamarellos-Bourboulis, and L. A. Joosten. 2012. Enhanced interleukin-1β production of PBMCs from patients with gout after stimulation with toll-like receptor-2 ligands and urate crystals. *Arthritis Res. Ther.* 14: R158.
20. Braga, T. T., M. F. Forni, M. Correa-Costa, R. N. Ramos, J. A. Barbuto, P. Branco, A. Castoldi, M. I. Hiyane, M. R. Davanso, E. Latz, et al. 2017. Soluble uric acid activates the NLRP3 inflammasome. *Sci. Rep.* 7: 39884.
21. Kim, S. M., S. H. Lee, Y. G. Kim, S. Y. Kim, J. W. Seo, Y. W. Choi, D. J. Kim, K. H. Jeong, T. W. Lee, C. G. Ihm, et al. 2015. Hyperuricemia-induced NLRP3 activation of macrophages contributes to the progression of diabetic nephropathy. *Am. J. Physiol. Renal Physiol.* 308: F993–F1003.
22. Sautin, Y. Y., T. Nakagawa, S. Zharikov, and R. J. Johnson. 2007. Adverse effects of the classic antioxidant uric acid in adipocytes: NADPH oxidase-mediated oxidative/nitrosative stress. *Am. J. Physiol. Cell Physiol.* 293: C584–C596.
23. Khosla, U. M., S. Zharikov, J. L. Finch, T. Nakagawa, C. Roncal, W. Mu, K. Krotova, E. R. Block, S. Prabhakar, and R. J. Johnson. 2005. Hyperuricemia induces endothelial dysfunction. *Kidney Int.* 67: 1739–1742.
24. Park, J. H., Y. M. Jin, S. Hwang, D. H. Cho, D. H. Kang, and I. Jo. 2013. Uric acid attenuates nitric oxide production by decreasing the interaction between endothelial nitric oxide synthase and calmodulin in human umbilical vein endothelial cells: a mechanism for uric acid-induced cardiovascular disease development. *Nitric Oxide* 32: 36–42.
25. Choi, Y. J., Y. Yoon, K. Y. Lee, T. T. Hien, K. W. Kang, K. C. Kim, J. Lee, M. Y. Lee, S. M. Lee, D. H. Kang, and B. H. Lee. 2014. Uric acid induces endothelial dysfunction by vascular insulin resistance associated with the impairment of nitric oxide synthesis. *FASEB J.* 28: 3197–3204.
26. Liang, W. Y., X. Y. Zhu, J. W. Zhang, X. R. Feng, Y. C. Wang, and M. L. Liu. 2015. Uric acid promotes chemokine and adhesion molecule production in vascular endothelium via nuclear factor-kappa B signaling. *Nutr. Metab. Cardiovasc. Dis.* 25: 187–194.
27. Scheepers, L. E. J. M., L. T. H. Jacobsson, S. Kern, L. Johansson, M. Dehlin, and I. Skoog. 2019. Urate and risk of Alzheimer's disease and vascular dementia: a population-based study. *Alzheimers Dement.* 15: 754–763.
28. Itahana, Y., R. Han, S. Barbier, Z. Lei, S. Rozen, and K. Itahana. 2015. The uric acid transporter SLC2A9 is a direct target gene of the tumor suppressor p53 contributing to antioxidant defense. *Oncogene* 34: 1799–1810.
29. Komori, H., K. Yamada, and I. Tamai. 2018. Hyperuricemia enhances intracellular urate accumulation via down-regulation of cell-surface BCRP/ABCG2 expression in vascular endothelial cells. *Biochim. Biophys. Acta Biomembr.* 1860: 973–980.
30. Hink, H. U., N. Santanam, S. Dikalov, L. McCann, A. D. Nguyen, S. Parthasarathy, D. G. Harrison, and T. Fukai. 2002. Peroxidase properties of extracellular superoxide dismutase: role of uric acid in modulating in vivo activity. *Arterioscler. Thromb. Vasc. Biol.* 22: 1402–1408.
31. Kilkenny, C., W. J. Browne, I. C. Cuthill, M. Emerson, and D. G. Altman. 2010. Improving bioscience research reporting: the ARRIVE guidelines for reporting animal research. *PLoS Biol.* 8: e1000412.
32. Preitner, F., A. Laverriere-Loss, S. Metref, A. Da Costa, C. Moret, S. Rotman, D. Bazin, M. Daudon, C. Sandt, A. Dessombz, and B. Thorens. 2013. Urate-induced acute renal failure and chronic inflammation in liver-specific Glut9 knockout mice. *Am. J. Physiol. Renal Physiol.* 305: F786–F795.
33. Schauer, C., C. Janko, L. E. Munoz, Y. Zhao, D. Kienhöfer, B. Frey, M. Lell, B. Manger, J. Rech, E. Naschberger, et al. 2014. Aggregated neutrophil extracellular traps limit inflammation by degrading cytokines and chemokines. *Nat. Med.* 20: 511–517.
34. Ma, Q., S. Steiger, and H. J. Anders. 2017. Sodium glucose transporter-2 inhibition has no renoprotective effects on non-diabetic chronic kidney disease. *Physiol. Rep.* 5: e13228.
35. Lech, M., and H. J. Anders. 2014. Expression profiling by real-time quantitative polymerase chain reaction (RT-qPCR). *Methods Mol. Biol.* 1169: 133–142.
36. Nakazawa, D., S. V. Kumar, J. Marschner, J. Desai, A. Holderied, L. Rath, F. Kraft, Y. Lei, Y. Fukasawa, G. W. Moeckel, et al. 2017. Histones and neutrophil extracellular traps enhance tubular necrosis and remote organ injury in ischemic AKI. *J. Am. Soc. Nephrol.* 28: 1753–1768.
37. Liu, S., Y. Yuan, Y. Zhou, M. Zhao, Y. Chen, J. Cheng, Y. Lu, and J. Liu. 2017. Phloretin attenuates hyperuricemia-induced endothelial dysfunction through co-inhibiting inflammation and GLUT9-mediated uric acid uptake. *J. Cell. Mol. Med.* 21: 2553–2562.
38. Kang, D. H., S. K. Park, I. K. Lee, and R. J. Johnson. 2005. Uric acid-induced C-reactive protein expression: implication on cell proliferation and nitric oxide production of human vascular cells. *J. Am. Soc. Nephrol.* 16: 3553–3562.
39. Eisenbacher, J. L., H. Schrezenmeier, B. Jahrsdörfer, C. Kaltenmeier, M. T. Rojewski, T. Yildiz, T. Beyer, A. Erle, D. S. Wiegmann, S. Grassl, et al. 2014. S100A4 and uric acid promote mesenchymal stromal cell induction of IL-10+/IDO+ lymphocytes. *J. Immunol.* 192: 6102–6110.
40. Lazzeri, E., M. L. Angelotti, A. Peired, C. Conte, J. A. Marschner, L. Maggi, B. Mazzinghi, D. Lombardi, M. E. Melica, S. Nardi, et al. 2018. Endocycle-related tubular cell hypertrophy and progenitor proliferation recover renal function after acute kidney injury. *Nat. Commun.* 9: 1344.
41. Bi, M., Q. Jiao, X. Du, and H. Jiang. 2018. Glut9-mediated urate uptake is responsible for its protective effects on dopaminergic neurons in Parkinson's disease models. *Front. Mol. Neurosci.* 11: 21.
42. Dower, K., D. K. Ellis, K. Saraf, S. A. Jelinsky, and L. L. Lin. 2008. Innate immune responses to TREM-1 activation: overlap, divergence, and positive and

negative cross-talk with bacterial lipopolysaccharide. *J. Immunol.* 180: 3520–3534.
43. Sieber, K. B., A. Batorsky, K. Siebenthall, K. L. Hudkins, J. D. Vierstra, S. Sullivan, A. Sur, M. McNulty, R. Sandstrom, A. Reynolds, et al. 2019. Integrated functional genomic analysis enables annotation of kidney genome-wide association study loci. *J. Am. Soc. Nephrol.* 30: 421–441.
44. Brovold, H., T. Lund, D. Svistounov, M. D. Solbu, T. G. Jenssen, K. Ytrehus, and S. N. Zykova. 2019. Crystallized but not soluble uric acid elicits pro-inflammatory response in short-term whole blood cultures from healthy men. *Sci. Rep.* 9: 10513.
45. Tung, Y. T., L. C. Lin, Y. L. Liu, S. T. Ho, C. Y. Lin, H. L. Chuang, C. C. Chiu, C. C. Huang, and J. H. Wu. 2015. Antioxidative phytochemicals from Rhododendron oldhamii Maxim. leaf extracts reduce serum uric acid levels in potassium oxonate-induced hyperuricemic mice. *BMC Complement. Altern. Med.* 15: 423.
46. Shi, Y. W., C. P. Wang, X. Wang, Y. L. Zhang, L. Liu, R. W. Wang, J. F. Ye, L. S. Hu, and L. D. Kong. 2012. Uricosuric and nephroprotective properties of Ramulus Mori ethanol extract in hyperuricemic mice. *J. Ethnopharmacol.* 143: 896–904.
47. Yang, Z., W. Xiaohua, J. Lei, T. Ruoyun, X. Mingxia, H. Weichun, F. Li, W. Ping, and Y. Junwei. 2010. Uric acid increases fibronectin synthesis through upregulation of lysyl oxidase expression in rat renal tubular epithelial cells. *Am. J. Physiol. Renal Physiol.* 299: F336–F346.
48. Romi, M. M., N. Arfian, U. Tranggono, W. A. W. Setyaningsih, and D. C. R. Sari. 2017. Uric acid causes kidney injury through inducing fibroblast expansion, Endothelin-1 expression, and inflammation. *BMC Nephrol.* 18: 326.
49. Preitner, F., A. Pimentel, S. Metref, C. Berthonneche, A. Sarre, C. Moret, S. Rotman, G. Centeno, D. Firsov, and B. Thorens. 2015. No development of hypertension in the hyperuricemic liver-Glut9 knockout mouse. *Kidney Int.* 87: 940–947.
50. Sil, P., H. Wicklum, C. Surell, and B. Rada. 2017. Macrophage-derived IL-1β enhances monosodium urate crystal-triggered NET formation. *Inflamm. Res.* 66: 227–237.
51. Kanellis, J., S. Watanabe, J. H. Li, D. H. Kang, P. Li, T. Nakagawa, A. Wamsley, D. Sheikh-Hamad, H. Y. Lan, L. Feng, and R. J. Johnson. 2003. Uric acid stimulates monocyte chemoattractant protein-1 production in vascular smooth muscle cells via mitogen-activated protein kinase and cyclooxygenase-2. *Hypertension* 41: 1287–1293.
52. Albertoni, G., and N. Schor. 2015. Resveratrol inhibits the intracellular calcium increase and angiotensin/endothelin system activation induced by soluble uric acid in mesangial cells. *Braz. J. Med. Biol. Res.* 48: 51–56.
53. Li, S., F. Zhao, S. Cheng, X. Wang, and Y. Hao. 2013. Uric acid-induced endoplasmic reticulum stress triggers phenotypic change in rat glomerular mesangial cells. *Nephrology (Carlton)* 18: 682–689.
54. Ryu, E. S., M. J. Kim, H. S. Shin, Y. H. Jang, H. S. Choi, I. Jo, R. J. Johnson, and D. H. Kang. 2013. Uric acid-induced phenotypic transition of renal tubular cells as a novel mechanism of chronic kidney disease. *Am. J. Physiol. Renal Physiol.* 304: F471–F480.
55. Tassone, E. J., A. Cimellaro, M. Perticone, M. L. Hribal, A. Sciacqua, F. Andreozzi, G. Sesti, and F. Perticone. 2018. Uric acid impairs insulin signaling by promoting Enpp1 binding to insulin receptor in human umbilical vein endothelial cells. *Front. Endocrinol. (Lausanne)* 9: 98.
56. Martinon, F., V. Pétrilli, A. Mayor, A. Tardivel, and J. Tschopp. 2006. Gout-associated uric acid crystals activate the NALP3 inflammasome. *Nature* 440: 237–241.
57. Ames, B. N., R. Cathcart, E. Schwiers, and P. Hochstein. 1981. Uric acid provides an antioxidant defense in humans against oxidant- and radical-caused aging and cancer: a hypothesis. *Proc. Natl. Acad. Sci. USA* 78: 6858–6862.
58. Whiteman, M., U. Ketsawatsakul, and B. Halliwell. 2002. A reassessment of the peroxynitrite scavenging activity of uric acid. *Ann. N. Y. Acad. Sci.* 962: 242–259.
59. Cantor, J. R., M. Abu-Remaileh, N. Kanarek, E. Freinkman, X. Gao, A. Louissaint, Jr., C. A. Lewis, and D. M. Sabatini, 2017. Physiologic medium rewires cellular metabolism and reveals uric acid as an endogenous inhibitor of UMP synthase. *Cell* 169: 258–272.e17
60. Iwata, H., S. Nishio, M. Yokoyama, A. Matsumoto, and M. Takeuchi. 1989. Solubility of uric acid and supersaturation of monosodium urate: why is uric acid so highly soluble in urine? *J. Urol.* 142: 1095–1098.
61. Manissorn, J., K. Fong-Ngern, P. Peerapen, and V. Thongboonkerd. 2017. Systematic evaluation for effects of urine pH on calcium oxalate crystallization, crystal-cell adhesion and internalization into renal tubular cells. *Sci. Rep.* 7: 1798.
62. Steiger, S., J. F. Grill, Q. Ma, T. Bäuerle, J. Jordan, M. Smolle, C. Böhland, M. Lech, and H. J. Anders. 2018. Anti-transforming growth factor β IgG elicits a dual effect on calcium oxalate crystallization and progressive nephrocalcinosis-related chronic kidney disease. *Front. Immunol.* 9: 619.
63. Mulay, S. R., O. P. Kulkarni, K. V. Rupanagudi, A. Migliorini, M. N. Darisipudi, A. Vilaysane, D. Muruve, Y. Shi, F. Munro, H. Liapis, and H. J. Anders. 2013. Calcium oxalate crystals induce renal inflammation by NLRP3-mediated IL-1β secretion. *J. Clin. Invest.* 123: 236–246.
64. Wilcox, W. R., and A. A. Khalaf. 1975. Nucleation of monosodium urate crystals. *Ann. Rheum. Dis.* 34: 332–339.
65. Martillo, M. A., L. Nazzal, and D. B. Crittenden. 2014. The crystallization of monosodium urate. *Curr. Rheumatol. Rep.* 16: 400.
66. Chhana, A., G. Lee, and N. Dalbeth. 2015. Factors influencing the crystallization of monosodium urate: a systematic literature review. *BMC Musculoskelet. Disord.* 16: 296.
67. Sakhaee, K., S. Nigam, P. Snell, M. C. Hsu, and C. Y. Pak. 1987. Assessment of the pathogenetic role of physical exercise in renal stone formation. *J. Clin. Endocrinol. Metab.* 65: 974–979.
68. Sakhaee, K., B. Adams-Huet, O. W. Moe, and C. Y. Pak. 2002. Pathophysiologic basis for normouricosuric uric acid nephrolithiasis. *Kidney Int.* 62: 971–979.
69. Pak, C. Y., K. Sakhaee, R. D. Peterson, J. R. Poindexter, and W. H. Frawley. 2001. Biochemical profile of idiopathic uric acid nephrolithiasis. *Kidney Int.* 60: 757–761.
70. Price, K. L., Y. Y. Sautin, D. A. Long, L. Zhang, H. Miyazaki, W. Mu, H. Endou, and R. J. Johnson. 2006. Human vascular smooth muscle cells express a urate transporter. *J. Am. Soc. Nephrol.* 17: 1791–1795.
71. Mobasheri, A., H. Dobson, S. L. Mason, F. Cullingham, M. Shakibaei, J. F. Moley, and K. H. Moley. 2005. Expression of the GLUT1 and GLUT9 facilitative glucose transporters in embryonic chondroblasts and mature chondrocytes in ovine articular cartilage. *Cell Biol. Int.* 29: 249–260.
72. Zhang, Y., T. Yamamoto, I. Hisatome, Y. Li, W. Cheng, N. Sun, B. Cai, T. Huang, Y. Zhu, Z. Li, et al. 2013. Uric acid induces oxidative stress and growth inhibition by activating adenosine monophosphate-activated protein kinase and extracellular signal-regulated kinase signal pathways in pancreatic β cells. *Mol. Cell. Endocrinol.* 375: 89–96.
73. Sabirov, R. Z., P. G. Merzlyak, T. Okada, M. R. Islam, H. Uramoto, T. Mori, Y. Makino, H. Matsuura, Y. Xie, and Y. Okada. 2017. The organic anion transporter SLCO2A1 constitutes the core component of the Maxi-Cl channel. *EMBO J.* 36: 3309–3324.
74. Bardin, T., and P. Richette. 2014. Definition of hyperuricemia and gouty conditions. *Curr. Opin. Rheumatol.* 26: 186–191.
75. Becker, M. A., H. R. Schumacher, Jr., R. L. Wortmann, P. A. MacDonald, D. Eustace, W. A. Palo, J. Streit, and N. Joseph-Ridge. 2005. Febuxostat compared with allopurinol in patients with hyperuricemia and gout. *N. Engl. J. Med.* 353: 2450–2461.
76. Dalbeth, N., M. E. House, O. Aati, P. Tan, C. Franklin, A. Horne, G. D. Gamble, L. K. Stamp, A. J. Doyle, and F. M. McQueen. 2015. Urate crystal deposition in asymptomatic hyperuricaemia and symptomatic gout: a dual energy CT study. *Ann. Rheum. Dis.* 74: 908–911.
77. Krishnan, E. 2012. Reduced glomerular function and prevalence of gout: NHANES 2009-10. *PLoS One* 7: e50046.